LARKMAN NUNATAK 06507 – INSIGHTS INTO THE IMPACT MELTING OF CARBONACEOUS CHONDRITES. Martin Schmieder[1,2], Barry J. Shaulis[1,2] and David A. Kring[1,2], [1]Lunar and Planetary Institute, 3600 Bay Area Boulevard, Houston, TX 77058, USA, schmieder@lpi.usra.edu, [2]NASA–SSERVI.

Introduction: The Antarctic meteorite Larkman Nunatak (LAR) 06507 is listed in the *Meteoritical Bulletin Database* as an LL-impact melt breccia [1,2]. As we will demonstrate, this meteorite represents a rare sample of a brecciated and shock-melt-veined CK-chondrite rather than an LL-impact melt breccia and, thus, provides insights into the impact-melting behavior of carbonaceous chondritic materials.

Sample and Analytical Methods: A polished 1" round thin section of meteorite split LAR 06507,9 (~11×12 mm) was investigated using optical microscopy at the LPI and a CAMECA SX-100 electron microprobe at the NASA Johnson Space Center (15 kV; 20 nA; 1–5 μm beam diameter).

Petrography and Geochemistry: A microscopic point count (n=3,101) indicates LAR 06507,9 is ~90% host rock breccia and ~10% shock-melt veins (Fig. 1a–c). The host rock is fine-grained, with hypidiomorphic olivine and pyroxene typically ≤200 μm and ≤100 μm in size, respectively. Olivine commonly exhibits planar fractures, more rarely mosaicism, and locally PDFs. In contrast to [1,2], who reported the presence of rare relict barred olivine chondrules in LAR 06507,2, the chondritic texture of LAR 06507,9 is barely discernible. The host rock contains ~81% silicates (olivine + pyroxene); ~8% plagioclase; ~9% magnetite; ~1% Fe,Ni-sulfide; ~1% voids and cracks; no metal. The shock melt domain is somewhat poorer in magnetite (~3%) and richer in sulfide microparticles (~5%). Because olivine and pyroxene are rather difficult to distinguish in optical microscopic analysis, a second point count (n=2,542) was done on a backscattered electron image of a representative portion of the host rock (~1.7×1.2 mm); olivine makes up ~70%; plagioclase ~14%; pyroxene ~6%; and primary oxide + sulfide ~10% of this sub-portion of the rock.

Olivine is $Fa_{34.0–35.3}$ (mean: $Fa_{34.6}$; wt% FeO/MnO = 133±15; atomic Fe/Mn =134±17; wt% NiO ~0.7–1.3; n=34) and is unzoned from crystal cores to rims. No low-Ca pyroxene was encountered. High-Ca-pyroxene is diopside: $Wo_{47.0–49.7}En_{38.0–42.2}Fs_{9.6–12.3}$ (mean: $Wo_{48.4}En_{40.2}Fs_{11.4}$; wt% FeO/MnO =136±58; atomic Fe/Mn = 130±54; with ≤0.2 wt% Cr_2O_3 and ≤0.5 wt% TiO_2; n=29) and is also unzoned. Pyroxene locally occurs as larger agglomerates of individual crystals. LAR 06507,9 contains numerous irregular-shaped 'pockets' of anhedral, polycrystalline, plagioclase a few to several hundred micrometers in size (Fig. 1b). The composition of plagioclase is, even within a single pocket, highly variable over a range of $Or_{0.2–5.5}Ab_{10.1–60.2}An_{36.7–89.7}$ (i.e., the pockets contain intermingled irregular subdomains of different plagioclase composition, within the range of andesine–bytownite), with subpercent concentrations of FeO (n=25). The texture and 'mottled' composition of these plagioclase pockets suggests they may represent recrystallized maskelynite: they poikilitically enclose grains of all other minerals identified in the rock; locally display polysynthetic twinning; lack vesicles; and contain irregular to locally conchoidal fractures (mainly in albite-rich regions). Plagioclase pockets are commonly the center of irregular radial fractures. Silicates are intergrown with accessory hypidiomorphic merrillite up to ~100 μm in crystal size (~3.5 wt% MgO; ~2.4 wt% Na_2O; ~0.06 wt% Y_2O_3; ~0.05 wt% SmO; with La_2O_3 and Ce_2O_3 near the detection limit; and F and Cl below detection limit; n=6). Opaques are predominantly magnetite: $Mag_{86}Chr_8Hc_6$ (~5.3 wt% Cr_2O_3; ~2.6 wt% Al_2O_3; ~0.4 wt% TiO_2; ~0.4 wt% NiO; ~0.2 wt% MgO; ~0.16 wt% V_2O_3; n=7; Fig. 1d). Aggregates of magnetite reach ~500 μm in size. Magnetite commonly hosts exsolution lamellae of ilmenite, more rarely Fe-Mg-Si-Al-rich melt veinlets in cracks, and is locally associated with an alteration phase (hematite?). In places, magnetite has been disintegrated into smaller, granular aggregates of polygonal crystallites, similar in texture to shocked chromite. Two intergrown Fe,Ni-sulfide phases were identified, pentlandite (~39–40 wt% Ni; ~32–33 wt% S; n=10) and monosulfide solid solution (~35–37 wt% Ni, ~35–38 wt% S; n=12; Fig. 1d), which occur as particles ≤200 μm in size.

Sample LAR 06507,9 is cross-cut by a number of melt veins up to several hundred micrometers thick (Fig. 1b;c). These have an olivine-dominated groundmass and are enriched in Al, Ca, and Na (up to ~9.8 wt% Al_2O_3; ~2–4 wt% CaO; ~0.8 wt% NiO; ~0.6 wt% Na_2O; ~0.3 wt% Cr_2O_3; ~0.1 wt% TiO_2; n=6), carry abundant microparticles (<5 μm) of silicate, magnetite, and Fe,Ni-sulfide, and commonly exhibit subparallel fractures perpendicular to the vein direction. Thin melt veins cross-cut larger olivine and pyroxene crystals, as well as irregular plagioclase pockets, and locally form micrometer-scale melt networks. Weathering of LAR 06507,9 corresponds to grade wi-1[3], as indicated by slight staining of silicates. Sulfide is locally replaced by an alteration phase similar in composition to jarosite (~6 wt% K_2O; ~31 wt% SO_3; ~46 wt% Fe_2O_3), which may have formed during terrestrial weathering.

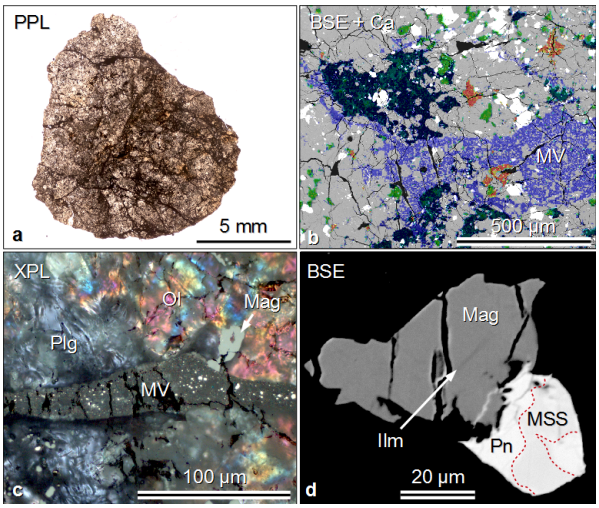

Fig. 1: Larkman Nunatak 06507,9. **(a)** Optical microscopic image of the brecciated CK-chondrite with a network of dark melt veins (plane-polarized light). **(b)** Backscattered electron (BSE) image and Ca-map overlay of host rock domain cross-cut by a melt vein (MV), distinguishing olivine (light gray), diopside (light green), plagioclase (dark blue-green), melt vein matrix (lighter blue), merrillite (red), and magnetite and Fe–Ni-sulfide (both white). **(c)** Optical image (cross-polarized + reflected light) of thin melt vein running across the host rock domain (Mag: magnetite; Ol: olivine; Plg: plagioclase). **(d)** BSE image of magnetite (Ilm: ilmenite exsolution lamella) and pentlandite (Pn) intergrown with monosulfide solid solution (MSS).

Interpretation and Discussion: Based on the petrologic characteristics, LAR 06507 appears to be a breccia cross-cut by a network of silicate shock-melt veins, produced from a CK6 (Karoonda-type) carbonaceous chondritic precursor that had previously largely lost the delineation of its chondrules through thermal metamorphism. LAR 06507 fulfills a series of criteria that are characteristic of CK-chondrites of higher-grade petrologic types: (1) the virtual lack of Fe,Ni-metal; (2) the ubiquity of magnetite (~5–8%), indicative of formation of the CK-chondrites under strongly oxidizing conditions; (3) a characteristic MgO vs. Cr_2O_3 signature for magnetite in CK4–6 chondrites; (4) equilibrated silicates; (5) olivine close to $Fa_{31\pm3}$, high in Ni; (6) a typical high Fe/Mn >100 in olivine and pyroxene; and (7) highly heterogeneous plagioclase domains [4–9]. Classified here as a shocked CK6 chondrite, LAR 06507 is potentially paired with one or more shock-veined CK6 chondrites collected in the same area in Antarctica, such as LAR 06636 and/or LAR 06869/72/73, all of which are characterized by similar modal and geochemical compositions [1,10–12].

The overall aspect of shock-veined LAR 06507,9 suggests a rather high shock stage (probably S5; ~30–55 GPa), corresponding to the formation of maskelynite from plagioclase (now recrystallized [13]) and pervasive formation of melt veins [14,15]; no ringwoodite was identified in the melt veins. We point out that the origin of compositionally heterogeneous plagioclase domains in CK chondrites, as seen in LAR 06507,9, is still a matter of debate (i.e., shock vs. thermal metamorphic vs. nebular origin, or combinations of different processes [16–20]).

Scott et al. [15] noted that, in comparison with ordinary chondrites, carbonaceous chondrites are characterized by lower levels of shock, up to stage S4 (~20–35 GPa; mosaicism in olivine [14]). However, some CK5- and CK6-chondrites (e.g., Elephant Moraine 83311) show evidence for stronger shock and melting [15]. Accordingly, [16] suggested intense shock recorded in some of the CK-chondrites (followed by annealing), perhaps implying a location closer to the Sun than CI and CM chondrites (see also [21]), where impact velocities are higher; while [18] pointed out that melting may have occurred at relatively mild shock pressures if the target asteroid was hot at the time of impact. Moreover, high porosity of most carbonaceous chondrites [22] may, through the collapse of pore space during shock, generate local pressure peaks and, thereby, facilitate localized melt production at comparatively low pressures [23].

Although CK and CV chondrites may share a common parent body [9], we note that the petrology of melt zones observed in the shocked CK chondrite LAR 06507 differs from those of CV- and CM-chondritic impact melt clasts [24]. This could be an effect of the difference in petrophysical and mineralogical properties between the anhydrous, strongly metamorphosed, CK6 chondrites and the more volatile-rich CV-chondrites of low-grade petrologic types, or a difference in their radial distance from the Sun.

References: [1] Weisberg M. K. et al. (2010) MB 98, *MAPS, 45*, p. 1546. [2] Satterwhite C. and Righter K. (2010, Eds.) *AMN, 33(1)*, p. 18. [3] Rubin A. E and Huber H. (2005) *MAPS, 40*, 1123–1130. [4] Kallemeyn G. W. et al. (1991) *GCA, 55*, 881–892. [5] Noguchi T. (1993) *Proc. NIPR Symp. Ant. Met., 6*, 204–233. [6] Geiger T. and Bischoff A. (1995) *PSS, 43*, 485–498. [7] Goodrich C. A. and Delaney J. S. (2000) *GCA, 64*, 149–160. [8] Neff K. E. and Righter K. (2006) LPS XXXVII, abstr. #1320. [9] Greenwood R. C. et al. (2010) *GCA, 74*, 1684–1705. [10] Satterwhite C. and Righter K. (2009, Eds.) *AMN, 32(2)*, p. 15. [11] Weisberg M. K. et al. (2008) MB 94, *MAPS, 43*, p. 1583. [12] Satterwhite C. and Righter K. (2008, Eds.) *AMN, 31(1)*, p. 25. [13] Ostertag R. and Stöffler D. (1982) *JGR, 87*, A457–A463. [14] Stöffler D. et al. (1991) *GCA, 55*, 3845–3867. [15] Scott E. R. D. et al. (1992) *GCA, 56*, 4281–4293. [16] Rubin A. E. (1992) *GCA, 56*, 1705–1714. [17] Ivanova M. A. et al. (2000) *MAPS, 35*, A83. [18] Tomeoka K. et al. (2005) *J. Mineral. Petrol. Sci., 100*, 116–125. [19] Nakamuta Y. et al. (2006) *J. Mineral. Petrol. Sci.*, 101, 308–318. [20] Chaumard N. and Devouard B. (2015) LPS XLVI, abstr. #1924. [21] Chaumard N. et al. (2012) *Icarus, 220*, 65–73. [22] Macke R. J. et al. (2011) *MAPS, 46*, 1842–1862. [23] Kowitz A. et al. (2013) *EPSL, 384*, 17–26. [24] Lunning N. G. et al. (2015) LPS XLVI, abstr. #2076.